NASA CR-152,013

THE EFFECT OF THE LIQUID-SOLID SYSTEM PROPERTIES ON THE INTERLINE HEAT TRANSFER COEFFICIENT

AUGUST 1977

Prepared under NASA P.O. # A-38597-B(DG)

by

P. C. WAYNER, JR.

DEPARTMENT OF CHEMICAL AND ENVIRONMENTAL ENGINEERING

RENSSELAER POLYTECHNIC INSTITUTE

TROY, N. Y. 12181

Prepared for

Ames Research Center
National Aeronautics and Space Administration
Moffett Field, California 94035

Abstract

A theoretical procedure to determine the heat transfer characteristics of the interline region of an evaporating meniscus using the macroscopic optical and thermophysical properties of the system is outlined. The analysis is based on the premise that the interline transport processes are controlled by the London-van der Waals forces between condensed phases (solid and liquid). The procedure is used to compare the relative size of the interline heat sink of various systems using a constant heat flux model. This solution demonstrates the importance of the interline heat flow number, $\overline{A}\, h_{fg}\, \nu^{-1}$, which is evaluated for various systems. The heat transfer characteristics of the decane-steel system are numerically compared with those of the carbon tetrachloride-quartz system. In order to evaluate the theoretical models and obtain direction for their refinement, the length of the interline region and the stability of the meniscus should be experimentally determined as a function of the heat flux and the interline heat flow number.

Contents

Nomenclature

$\bar{A}$, dispersion constant [J];

A, Hamaker constant [see Eq. (III.2)] [J];

D, mean separation between close packed planes [m];

G, constant in equation (II.5) [m^{-2}];

$\hbar 2\pi$, Planck's constant (J·s];

h, heat-transfer coefficient [$W \cdot m^{-2} \cdot K^{-1}$];

h_{fg}, latent heat of vaporization [$J \cdot kg^{-1}$];

K, constant in Eq. [III.18];

K, curvature [m^{-1}];

k, thermal conductivity [$W \cdot m^{-1} \cdot K^{-1}$];

k, adsorption constant;

M, molecular weight [$kg \cdot mol^{-1}$];

$\dot{m}$, mass flux [$kg \cdot m^{-2} \cdot s^{-1}$];

n, refractive index;

P, pressure [$N \cdot m^{-2}$];

Q, heat transferred [$W \cdot m^{-1}$];

q, heat flux [$W \cdot m^{-2}$];

R, universal gas constant [$J \cdot mol^{-1} \cdot K^{-1}$];

R, radius of meniscus [m];

S, solid thickness [m];

T, temperature [K];

U, overall heat transfer coefficient, [$W \cdot m^{-2} \cdot K^{-1}$];

u, velocity [$m \cdot s^{-1}$];

v, molar volume [$m^3 \cdot mol^{-1}$];

Greek Symbols

β, see Eq. (III.2);

Γ, adsorbed per unit area [$mol \cdot m^{-2}$];

γ, dimensionless heat-transfer coefficient;

γ, interfacial free energy, [$J \cdot m^{-2}$];

δ, film thickness [m];

ε, dielectric constant, $\varepsilon = \varepsilon' + i\varepsilon''$;

η, dimensionless film thickness;

θ, contact angle, [degrees];

μ, absolute viscosity [$kg \cdot m^{-1} \cdot s^{-1}$];

Greek Symbols (continued)

ν, kinematic viscosity [$m^2 \cdot s^{-1}$];

ξ, dimensionless film length coordinate;

ξ, imaginary part of complex frequency [$rad \cdot s^{-1}$];

π, defined by Eq. [III.13];

ρ, density [$kg \cdot m^{-3}$];

σ, evaporation coefficient [dimensionless];

$\bar{\omega}$, defined by Eq. (III.4) [$rad \cdot s^{-1}$];

ω, angular frequency [$rad \cdot s^{-1}$];

Subscripts

E, evaporating;

e, evaporative;

ℓ, liquid phase;

ℓv, liquid-vapor interface;

NE, non-evaporating;

s, solid;

O, evaluated at interline;

v, vapor phase;

Superscripts

d, dispersion;

-, averaged;

id, ideal;

*, differentiation with respect to ξ;

^, complex index of refraction;

I. Introduction

In the analysis of heat pipes it has been common practice to use a liquid transport number, $N = \gamma h_{fg}/\nu$, to evaluate the heat sink capability of the evaporating meniscus. In addition, the understanding of the evaporating meniscus can be enhanced by defining a "meniscus shape factor", $R(K_E - K_{NE})$, which is the product of the radius of the capillary and the change in average curvature of the evaporating meniscus (1). This shape factor accounts for the fact that liquid flows as a result of a change in the meniscus shape. Although these two groups aid our understanding of the evaporating meniscus, they do not describe the transport processes occurring in the interline region (junction of solid, evaporating meniscus and vapor). The analysis of the evaporating meniscus is extended herein to the interline region by evaluating the effect of the London-van der Waals forces between the solid and liquid on the pressure in the liquid and on the vapor pressure of the liquid. This analysis is based on the premise that the interline transport processes are ultimately controlled by the dispersion forces resulting from the electromagnetic fields of the solid and liquid. This effect becomes important when the thickness of the liquid is less than 10^{-7}m. Since this region is relatively short in extent, it accounts for approximately 10% of the evaporation process. However, since this is the location where the meniscus "hangs on to the solid", the stability of the meniscus is probably determined in this region. In addition, the contact angle fixes the extent of the meniscus. Therefore, the region is of critical importance.

In order to quantify the effect of the liquid-solid system properties on the interline heat transfer coefficient a solution for a constant heat flux model of the interline region is obtained in Section II. This solution demonstrates the importance of the group of properties $\bar{A} h_{fg}/\nu$, which we

call the interline heat flow number. This replaces the liquid transport number, $\gamma h_{fg}/\nu$, as the important transport group in the interline region where the dispersion constant, $\bar{A}$, is more important than the surface tension, γ .

Assuming that bulk values can be used for the heat of vaporization and the kinematic viscosity, the interline heat flow number can be evaluated if values for $\bar{A}$ are obtainable. This problem is addressed below in Section III. The literature on London-van der Waals forces has been searched and procedures to determine the dispersion constant $\bar{A}$ are presented. Numerical values of the theoretical interline heat flow number and the interline heat sink are then determined and discussed for wetting systems.

In Section IV, the theoretical interline heat sink is determined for various liquid-solid systems. These results demonstrate the use of a procedure whereby the basic macroscopic optical (electromagnetic) properties of the liquid-solid system can be used to predict and compare the heat transfer characteristics of the evaporating meniscus in the interline region.

II. Constant Heat Flux Model for Interline Region

In a previous paper (2), a procedure to determine the theoretical heat transfer coefficient for the interline region (junction of vapor, adsorbed evaporating thin film and adsorbed non-evaporating thin film) of a wetting film was developed. Since the analysis was based on the assumption of a constant liquid-vapor interfacial temperature, the effect of the thermal conducitivity of the solid on the process was not included. Herein, an approximate procedure to determine the heat sink capability of the interline region is developed in which the effect of the solid resistance to heat transfer is included. The formulation uses a simple one-dimensional constant heat flux model. Although the general approach used in Ref. (2) is continued, the solution herein is directed towards a limiting case in which the solid conductance is controlling. Since the value of the ideal liquid-vapor interfacial heat transfer coefficient is very large, solid conductance is found to dominate the overall heat transfer coefficient in the interline region after a small increase in the film thickness. The formulation allows the relative effect of the overall heat transfer coefficient and the "surface transfer coefficient" to be evaluated. The results are useful for predicting and comparing the heat sink capability of various liquid-solid systems for use in compact heat exchangers such as the grooved evaporator and the inverted meniscus heat pipe. An effective heat transfer coefficient is defined for this purpose. For a review of the prior literature the readers are directed to the extensive literature cited in Ref. (2).

II.1 Development of the Equations

The system to be studied consists of a thin, evaporating, adsorbed film of pure liquid on a horizontal solid substrate of thickness, S , (see Fig. II.1). The system is not drawn to scale in Fig. (II.1) since S>>x . The shape of the thin film is steady since the evaporating liquid is replenished by fluid flow towards the interline from a source outside of the analyzed region. The temperature of the solid surface at y = -S is a constant, T_s , which is greater than the vapor temperature, T_v . If the film is sufficiently thin, it is kept from evaporating by London-van der Waals dispersion forces between the solid and liquid. If a section of the film is slightly tapered, portions of the film may be sufficiently thick to allow evaporation. The junction between the non-evaporating and the evaporating thin film is the interline. Fluid flows in the negative "X" direction in the evaporating thin film as a result of a pressure gradient in the film resulting from the film thickness gradient.

Using the procedure developed in Ref. (2) the evaporative heat flux is

$$q = h_{fg}\,\dot{m}_e = \frac{h_{fg}\,\overline{A}}{\nu}\left(\frac{\delta'}{\delta}\right)' \qquad \text{(II.1)}$$

For the present case, q is assumed to be a constant, $\overline{q}$, and equal to the average macroscopic heat flux through the system:

$$U\,(T_s - T_v) = \frac{h_{fg}\,\overline{A}}{\nu}\left(\frac{\delta'}{\delta}\right)' \qquad \text{(II.2)}$$

where, the average overall heat transfer coefficient, U , is defined as

$$U = \left[\frac{S}{k_s} + \frac{\overline{\delta}}{k_\ell} + \frac{1}{\overline{h}_{\ell v}}\right]^{-1} \qquad \text{(II.3)}$$

in which, $\overline{h}_{\ell v}$ is the average liquid-vapor interfacial heat transfer coefficient and $\overline{\delta}$ is the average thickness of the thin film. This approximate macroscopic

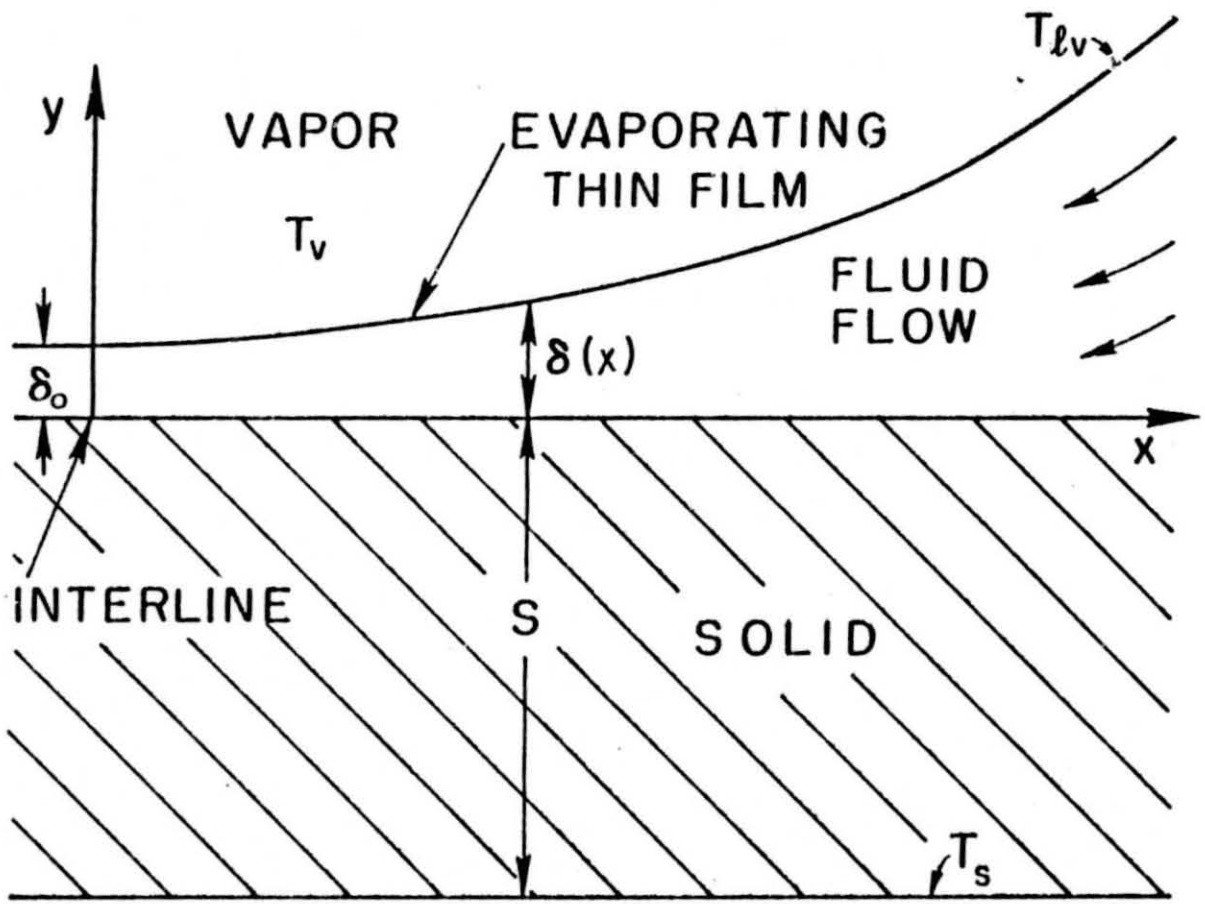

FIGURE (II.1) Interline junction of vapor, evaporating thin film and non-evaporating thin film on solid of thickness, S, (not drawn to scale).

formulation is primarily for the limiting case of $S/k_2 >> \bar{h}_{\ell v}^{-1}$. Eq. (II.2) is made dimensionless by using the previously defined variables (2):

$\eta = \delta/\delta_0$; $\xi^2 = G\,X^2$; $\eta^* = d\eta/d\xi$.

$$\left(\frac{\eta^*}{\eta}\right)^* = \frac{U\nu}{h_{fg}\,\bar{A}G}\left(T_s - T_v\right) \tag{II.4}$$

where

$$G = \frac{\nu}{\bar{A}}\left(\frac{2}{2-\sigma}\right)\left(\frac{M}{2\pi R\,\bar{T}}\right)^{1/2}\left(\frac{P_v\,M\,h_{fg}}{R}\right)\left(\frac{T_{\ell v} - T_v}{T_{\ell v}\,T_v}\right)_0 \tag{II.5}$$

and the interline thickness, δ_0 , is given by

$$\delta_0 = \sqrt[3]{\frac{\bar{A}\,V_\ell\,T_v}{M\,h_{fg}\,(T_{\ell v} - T_v)_0}} \quad . \tag{II.6}$$

Since

$$\frac{h_{fg}\,\bar{A}\,G}{\nu} = h_{\ell v}^{id}\,(T_{\ell v} - T_v)_0 = q^{id} \tag{II.7}$$

this group gives the ideal heat flux based on the kinetic theory of vapor flow that would occur at a liquid-vapor interface due to the temperature differences, $(T_{\ell v} - T_v)_0$. Using Eqs. (II.4 - II.7) gives

$$\left(\frac{\eta^*}{\eta}\right)^* = \frac{\bar{q}}{q^{id}} = \bar{\gamma} \quad . \tag{II.8}$$

The dimensionless average heat flux, $\bar{\gamma}$, can also be written as

$$\bar{\gamma} = \frac{\left(T_s - T_v\right)}{\left(T_{\ell v} - T_v\right)_0}\left[\frac{S\,h_{\ell v}^{id}}{k_s} + \frac{\bar{\delta}\,h_{\ell v}^{id}}{k_\ell} + \frac{h_{\ell v}^{id}}{\bar{h}_{\ell v}}\right]^{-1} \tag{II.9}$$

which explicitly includes the sum of the three relative resistances to heat transfer in the system: solid/ideal liquid-vapor interface; liquid film/ideal

liquid-vapor interface; liquid-vapor interface/ideal liquid-vapor interface. In Ref. (2), $T_s \to T_{\ell v}$, $k_s \to \infty$, $\bar{\delta}\, h^{id}_{\ell v}/k_\ell \to 0$ and $\bar{\gamma} = \bar{h}_{\ell v}/h^{id}_{\ell v}$. For this limit with a variable heat flux, the heat flux ratio depends on the extent of the zone of evaporation, $\xi(\eta)$, $\bar{\gamma} = 0.5\ (\eta^{-1} + \eta^{-2})$. Solving Eq. (II.8) for constant $\bar{\gamma}$ with the boundary conditions:

$$\eta(0) = 1 \tag{II.10a}$$

$$\frac{d\eta}{d\xi}\Big|_0 = \eta_0^* \tag{II.10b}$$

we obtain

$$\ell n\ (\eta) = \frac{\bar{\gamma}\,\xi^2}{2} + \eta_0^*\,\xi \tag{II.11}$$

For the present case, the dimensionless contact angle is taken to be zero, $\eta_0^* = 0$, and the extent of the region of evaporation, ξ , is

$$\xi = \left[\frac{2\ \ell n\ \eta}{\bar{\gamma}}\right]^{0.5} \tag{II.12}$$

or

$$x = \left[\frac{2\ \ell n\ \eta}{G\ \bar{\gamma}}\right]^{0.5} = \left[\frac{2\ h_{fg}\ \bar{A}\ \ell n\ \eta}{\bar{q}\ \nu}\right]^{0.5} \tag{II.13}$$

The size of the interline heat sink, Q , with a film thickness, $\eta \geq 1$, is

$$Q = \bar{q}\ x = q^{id}\left[\frac{2\ \bar{\gamma}\ \ell n\ \eta}{G}\right]^{0.5} \tag{II.14}$$

Using the previous definitions, Eq. (II.14) becomes

$$Q = \left(2\ U\ h_{fg}\ \bar{A}\ (T_s - T_v)\ \nu^{-1}\ \ell n\ \eta\right)^{0.5} \tag{II.15a}$$

the solution for the limiting case of constant interfacial temperature (2) is

$$Q = h_{fg}\,\bar{A}\,G^{0.5}\,\nu^{-1}\,[1 - 0.5\,(\eta^{-1} + \eta^{-2})]\,\xi(\eta) \qquad \text{(II.15b)}$$

Eq. (II.15a) can be written various ways in order to emphasize different characteristics of the system. Rewriting Eq. (II.15a) as

$$Q = \bar{q}\,x = \left(\frac{h_{fg}\bar{A}}{\nu}\right)\left(\frac{2\,\ell n\,\eta}{x}\right) \qquad \text{(II.15c)}$$

demonstrates that the length x of the evaporating thin film is a measurable quantity which is inversely proportional to the interline heat sink, Q . We can also use these results to define an effective overall heat transfer, U_{eff}, as

$$U_{eff} = \left(\frac{2\dot{U}}{T_s - T_v}\right)^{0.5}\left(\frac{h_{fg}\,\bar{A}}{\nu}\right)^{0.5} \qquad \text{(II.15d)}$$

in which $U \tilde{\sim} k/S$.

II.2 Discussion of Theoretical Equations

Equation (II.13) gives the length of the evaporating film for given values of the dimensionless thickness, η , and the parameter $\frac{2\, h_{fg}\, \bar{A}}{\nu\, \bar{q}}$ in which $\bar{q} = U\,(T_s - T_v)$. In the limit of negligible heat flux, $(\bar{q} = 0)$, an infinite length of an adsorbed non-evaporating film of thickness δ_0 is present. In Eq. (II.3), $U = 0$ because $\bar{h}_{\ell v} = 0$. To compare the heat sink capability, Q, of various systems using Eq. (II.15a) with equal dimensionless thickness, η, the parameter, $[2\, U\, h_{fg}\, \bar{A}\, (T_s - T_v)/\nu]$, is important. This includes the usual dimensions of the system and the properties of the liquid and solid. In addition, it includes the dispersion constant, $\bar{A}$, which accounts for the London-van der Waals dispersion force between the solid and liquid. Therefore, the relative effect of the classical overall heat transfer coefficient, U, and the "surface transfer coeffcient", $\bar{A}/\nu$, can be evaluated. This also defines an effective heat transfer coefficient, $[2\, U\, \bar{A}\, h_{fg}/\nu(T_s - T_v)]^{0.5}$ based on the film thickness range $\eta > 1$. Further evaluation of Eq. (II.15) suggests that the important group is $\bar{A}\, h_{fg}/\nu$ which we name the "interline heat flow number". This gives the variation of the heat sink capability of a thin film of thickness range $\eta > 1$ as a function of the solid-liquid system for a fixed product of $U\, \Delta T = k\, \Delta T/S$. This important group is evaluated in Section III.

It is not possible to increase the heat flux without bound as suggested by the equations because the system would become unstable. This can be seen by rewriting Eq. (II.9) as

$$U\,(T_s - T_v) = \bar{\gamma}\,(T_{\ell v} - T_v)_0\, h^{id}_{\ell v} \qquad \text{(II.16)}$$

For the case of constant liquid-vapor interfacial temperature (negligible solid resistance) the heat flux ratio, $\bar{\gamma}$, has a limiting value of

$$\bar{\gamma} = 1 - 0.5\ (\eta^{-1} + \eta^{-2}) \qquad \text{(II.17)}$$

For the constant heat flux case, $\bar{\gamma}$, would be less than this value. The limit for the value of $(T_{\ell v} - T_v)_0$ depends on the ability of the evaporating film profile to change and provide the necessary pressure gradient for flow which is finite. This stability limit is discussed in Ref. (2).

In Figure (II.2), the dimensionless heat sink capability, $\bar{\gamma}\,\xi$, is presented as a function of the dimensionless thickness, η , for the following four cases: $\bar{\gamma} = 0.5$; $\bar{\gamma} = 0.25$; $\bar{\gamma} = 0.05$; $\bar{\gamma} = 1 - 0.5\ (\eta^{-1} + \eta^{-2})$. The value of the heat sink for the constant liquid-vapor interfacial temperature case starts below the constant heat flux case because of effect of the dispersion force on vapor pressure. However, it surpases the constant heat flux case at a very small dimensionless thickness. It is interesting to note that the value of $\bar{\gamma}\,\xi$ at $\eta = 1.1$ is approximately $0.25\ \bar{\gamma}\,\xi\ (\eta = 10)$ for $\bar{\gamma} = 0.25$. Therefore, the value of ξ at $\eta = 1.1$ is approximately $0.25\ \xi\ (\eta - 10)$. This emphasizes the result that the thickness of the thin film increases slowly at first and then progressively faster. The thin film profiles for three values of $\bar{\gamma}$ are also presented in Fig. (II.2). Comparing these profiles demonstrates the result that the thin film slope predicted by the constant interfacial temperature model is considerably smaller than that predicted by the constant heat flux model. Combining the results of the two limiting cases for a closer approximation of the real physical situation, we can say, qualitatively, that the initial portion of the evaporating thin film follows the constant temperature model until thermal resistance limits the heat flux to a constant value. This limit occurs at a very small thickness increase. Numerical examples of the interline heat sink are given later in Section IV. The interline heat flow number is evaluated in the next section.

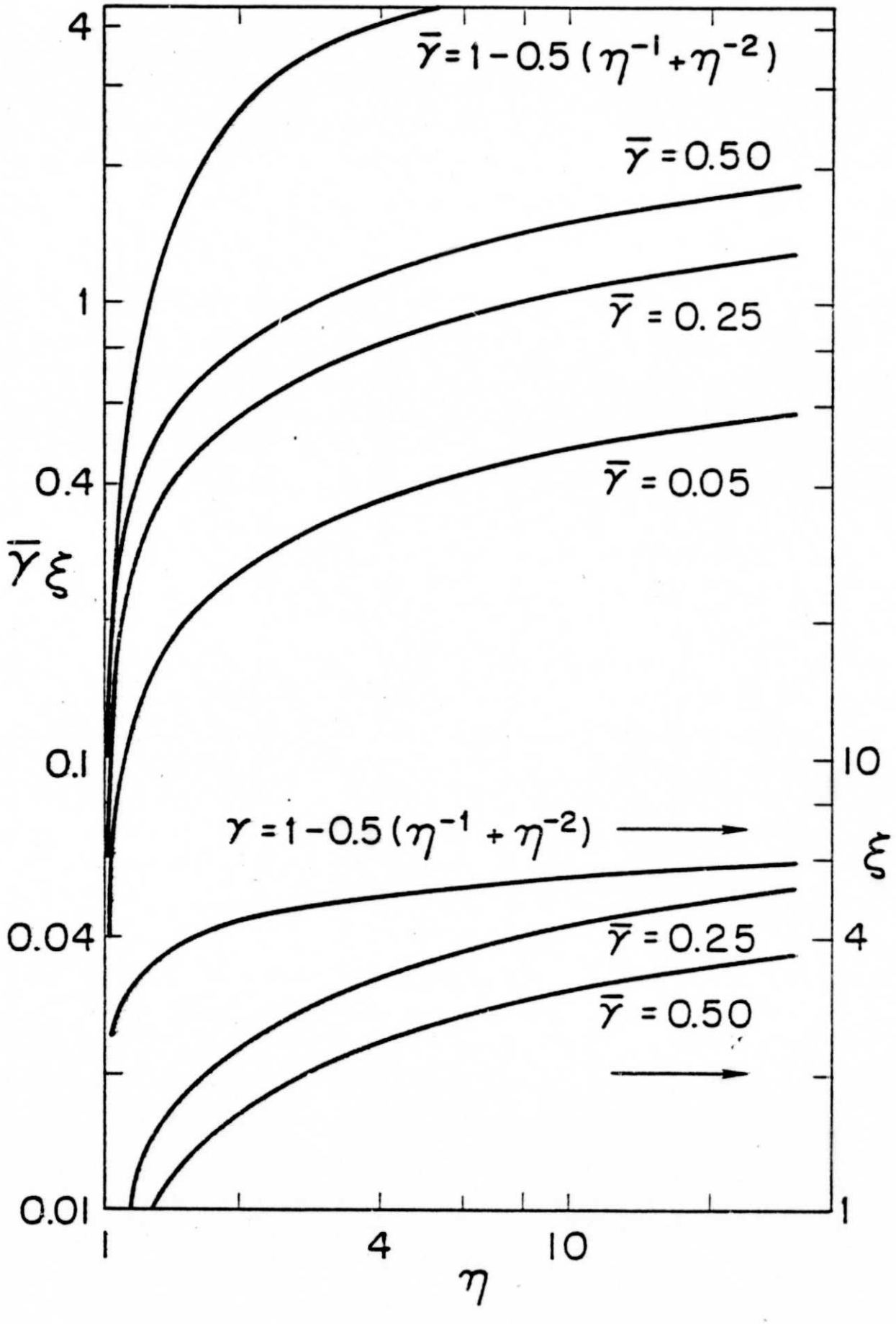

FIGURE (II.2) Dimensionless film profiles, ξ, and dimensionless heat sink capability profiles, $\bar{\gamma}\xi$, for various values of the dimensionless heat flux, $\bar{\gamma}$.

III. Evaluation of the Interline Heat Flow Number : $\bar{A}\, h_{fg}\, \nu^{-1}$

The objective of this project is to quantify the effect of the liquid-solid system properties on the interline heat transfer coefficient. In order to do this, an effective heat transfer coefficient has to be defined that includes both the solid conductance and a surface transfer coefficient for liquid flow, $\bar{A}/\nu$. As described above, this has been accomplished by using a constant heat flux model. The resulting effective heat transfer coefficient is found to be $[2\ U\ \bar{A}\ h_{fg}/\nu\ \Delta T]^{0.5}$. In this coefficient the Interline Heat Flow Number, $\bar{A}\ h_{fg}/\nu$, replaces the Liquid Transport Number, $\gamma\ h_{fg}/\nu$, as the important transport group. That is, the dispersion constant, $\bar{A}$, becomes important instead of the surface tension when the meniscus becomes sufficiently thin so that the solid effects the liquid properties. Having defined the heat transfer coefficient in this manner, the problem is reduced to evaluating the dispersion constant $\bar{A}$ which accounts for the London-van der Waals forces between condensed phases.

III.1 The Dispersion Constant, $\bar{A}$

For the purpose of this study we assume that the vapor pressure over an adsorbed film of liquid is a function of the temperature of the liquid and the net London-van der Waals force of attraction between the solid and liquid (2). The force of attraction between the solid and liquid can result in a lowering of the liquid vapor pressure, $P_{v\ell v}$, relative to the normal thermodynamic vapor pressure, $P_{v\ell vt}$, at the liquid temperature, $T_{\ell v}$. This vapor pressure lowering can be related to the dispersion force by the following equation:

$$\frac{R\,T_{\ell v}}{V_\ell}\,\ell n\,\frac{P_{v\ell v}}{P_{v\ell vt}} = -\frac{\bar{A}}{\delta^3} \qquad \text{(III.1)}$$

where δ is the thickness of the absorbed layer and $\bar{A}$ is the dispersion constant. In this case, $-\bar{A}/\delta^3$ represents the relative force of attraction per unit area between the vapor and solid across a film of liquid, ($\bar{A} > 0$). The van der Waals force of attraction between any two atoms or molecules may be divided into dispersion, induction and orientation forces. Orientation forces arise only in the case of polar molecules. A polar molecule may also induce polarity in a nearby neutral molecule and this results in an attractive induction force between them. With non-polar molecules or atoms the non-polarity is time average. At very short intervals the molecules and atoms are found to possess finite fluctuating dipole moments. These instantaneous moments result in an attractive force between the molecules or atoms by inducing polarity in neighboring atoms or molecules. The attractive force between condensed bodies (solid or liquid) resulting from these fluctuating electromagnetic fields can be described using the macroscopic optical properties of the materials and are called London-van der Waals dispersion forces. Except for the case of strongly polar molecules, the dispersion force generally dominates. Herein we will be mainly concerned with non-polar molecules. A good description of the development of the London-van der Waals force concept is given by Chu (3).

III.2 Calculation of the Dispersion Constant, $\bar{A}$

Basically, there are two methods of calculating the London-van der Waals dispersion force between condensed bodies. The microscopic approach starts with the interaction between individual atoms or molecules and postulates their additivity so that the attractive force between the macroscopic bodies can be calculated by integration over all atoms or molecules (4). The result is a product of a purely geometrical term and the Hamaker constant, $A_{s\ell v}$, which depends on the materials involved. The second method, the macroscopic approach developed by Lifshitz and co-workers (5), uses the macroscopic optical properties of the interacting macroscopic bodies and calculates the London-van der Waals dispersion force from the imaginary part of the complex dielectric constants. It appears to be generally accepted in the literature that the macroscopic approach is physically more satisfying than the microscopic approach. Presently we are concerned with a first order approximation of the adsorption effect on heat transfer. Therefore it is advantageous to use the results of both calculational methods in order to obtain maximum use of the previous literature. Where the results are different, preference will be given to the macroscopic approach.

When the molecules are an appreciable distance apart the fluctuating dipoles are no longer in phase since the time required for the electromagnetic field of one instantaneous dipole to reach a neighboring molecule and return may be comparable to the fluctuating field itself. In this case, the dependency of the force on distance changes from δ^{-3} to δ^{-4} and the interaction is known as the retarded London-van der Waals interaction. The transition is gradual. The case of small δ is of greater interest herein and we restrict ourselves to the non-retarded attraction.

A good physical description of the microscopic approach is given by

Sheludko (6). Using the microscopic procedure the equation for the temperature independent dispersion constant is

$$\bar{A} = \frac{A_{\ell s} - A_{\ell\ell}}{6\pi} = \div \frac{A_{s\ell v}}{6\pi} \qquad \text{(III.2)}$$

with

$$A_{\ell\ell} = \frac{\pi^2 \beta_{\ell\ell}}{\bar{v}_\ell^{\,2}} \qquad \text{and} \qquad A_{\ell s} = \frac{\pi^2 \beta_{\ell s}}{\bar{v}_\ell \bar{v}_s}$$

where $\bar{v}_i^{-1}$ is the number of atoms or molecules per unit volume and β_{ij} is the constant in London's equation for the attraction between two atoms. If the force of attraction between the liquid and solid (represented by $A_{\ell s}$) is greater than the force of attraction between two liquid molecules (represented by $A_{\ell\ell}$) the liquid wets the solid and a decrease in the vapor pressure occurs.

Using the macroscopic procedure, an equivalent Hamaker constant, $A_{s\ell v}$, can be obtained from the Lifshitz-van der Waals constant, $\hbar\,\bar{\omega}_{s\ell v}$:

$$A_{s\ell v} = \frac{3\,\hbar\,\bar{\omega}_{s\ell v}}{4\pi} \qquad \text{(III.3)}$$

Using this definition to relate both approaches through an equivalent Hamaker constant, the two procedures can be unified and compared.

For the purpose of this report the Lifshitz-van der Waals constant can be calculated using the following approximate formula (5):

$$\bar{\omega}_{s\ell v} = \int_0^\infty \frac{[\varepsilon_\ell(i\xi) - \varepsilon_s(i\xi)]\,[\varepsilon_\ell(i\xi) - 1]}{[\varepsilon_\ell(i\xi) + \varepsilon_s(i\xi)]\,[\varepsilon_\ell(i\xi) + 1]}\, d\xi \qquad \text{(III.4)}$$

where ε_s, ε_v, ε_ℓ are the frequency dependent dielectric constants of the solid, vapor ($\varepsilon_v = 1$), and liquid evaluated along the imaginary frequency axis, $i\xi$. (The assumptions associated with deriving this equation from a more general formulation are presented in Reference 5.) In turn these imaginary frequency dependent dielectric constants can be calculated from the imaginary part of the

complex dielectric constant which can be experimentally measured. The dielectric constant, $\varepsilon(\omega)$, is a complex function of the frequency, ω.

$$\varepsilon(\omega) = \varepsilon'(\omega) + i\,\varepsilon''(\omega) \qquad \text{(III.5)}$$

The function $\varepsilon(\omega)$ is related to the complex index of refraction, $\hat{n}$, the refractive index, n , and the absorption constant, k, by

$$\sqrt{\varepsilon(\omega)} = \hat{n} = n(\omega) + i\,k(\omega) \qquad \text{(III.6)}$$

$$\varepsilon'(\omega) = n^2(\omega) - k^2(\omega) \qquad \text{(III.7)}$$

$$\varepsilon''(\omega) = 2n(\omega)\,k(\omega) \qquad \text{(III.8)}$$

For the purpose of analysis, it is useful to consider the frequency, ω , to be a complex variable:

$$\omega = \omega' + i\xi \qquad \text{(III.9)}$$

As presented above, the dispersion force depends only on the value of the dielectric constant on the imaginary frequency axis, $\varepsilon(i\xi)$. The function is always positive and is related to the dissipation of energy in an electromagnetic wave propagated in the medium. $\varepsilon(i\xi)$ is a real quantity which decreases monotonically from ε_o (the electrostatic dielectric constant) $\varepsilon_o = \hat{n}^2 > 1$ for dielectrics or from $+\infty$ for ideal metals at $\omega = i0$ to 1 at $\omega = i\infty$ for all materials (7). Without the need for a specific model, the Kramers-Kronig relations can be used to calculate $\varepsilon(i\xi)$ from the imaginary part of the dielectric constant, $\varepsilon''(\omega)$, (7).

$$\varepsilon(i\xi) = 1 + \frac{2}{\pi}\int_0^\infty \frac{X\,\varepsilon''(X)}{(X^2 + \xi^2)}\,dX \qquad \text{(III.10)}$$

where ξ and X are angular frequencies of the electromagnetic field. Therefore,

$\varepsilon(i\xi)$ can be obtained directly from experimental data on the refractive index and adsorption constant. However, due to the lack of sufficient data for the frequency dependent optical constants, semi-empirical models are usually used. On the other hand, due to the basic importance of optical data in many fields, there is a wealth of procedures and models available in the literature. In addition, the volume of available data is also rapidly expanding..

III.3 Contact Angle

For the purpose of completeness, it is desirable to address the related topics of contact angle and surface tension. The Young-Dupré equation for the contact angle between a liquid, ℓ , and a solid surface, s, is (8)

$$\gamma_\ell \cos \theta = \gamma_{sv} - \gamma_{\ell s} \qquad \text{(III.11)}$$

In general, $\gamma = \gamma^d + \Sigma_m \gamma_m$, in which γ^d is the contribution to surface tension resulting from the dispersion forces and $\Sigma_m \gamma_m$ are the contributions due to other interactions (dipole-dipole, metallic, etc.). The surface free energy of the solid-vapor interface, γ_{sv} , is related to the surface free energy of the uncontaminated surface by [papers in (9) discuss this material]

$$\gamma_{sv} = \gamma_s - \pi_e \qquad \text{(III.12)}$$

The difference between these two surface free energies is the decrease in the surface free energy of the solid surface, π_e , resulting from adsorption

$$\pi_e = RT \int_0^{P_v} \Gamma \, d \, \ell n \, P_v \qquad \text{(III.13)}$$

If the interaction between the solid and liquid is by dispersion forces only, the solid-liquid interfacial free energy can be represented by

$$\gamma_{\ell s} = \gamma_\ell + \gamma_s - 2\sqrt{\gamma_\ell^d \gamma_s^d} \qquad \text{(III.14)}$$

Combining these equations with $\pi_e \tilde{\simeq} 0$ gives

$$\gamma_\ell (1 + \cos \theta) = 2\sqrt{\gamma_\ell^d \gamma_s^d} \qquad \text{(III.15)}$$

Finally, the expression for the contact angle becomes

$$\cos \theta = 2\sqrt{\frac{\gamma_\ell^d \gamma_s^d}{\gamma_\ell^2}} - 1 \qquad \text{(III.16)}$$

In general, the contact angle can be related to the Hamaker constant by using

$$\gamma_\ell^d = K_{\ell\ell}\, A_{\ell\ell} \qquad \text{(III.17)}$$

in which $K_{\ell\ell}$ is a constant related to the molecular dimensions. Using Eqs. (III.17) and (III.16) for a system in which $\gamma_\ell = \gamma_\ell^d$ we obtain

$$\cos\theta = 2\sqrt{\frac{A_{ss}\, K_{ss}}{A_{\ell\ell}\, K_{\ell\ell}}} - 1 \qquad \text{(III.18)}$$

If $A_{ss}\, K_{ss} > A_{\ell\ell}\, K_{\ell\ell}$, $\theta = 0$, and the liquid forms a stable wetting film on the solid surface. These assumptions apply to the simple system of a non-polar fluid interacting with a surface through dispersion forces: e.g., an n-alkane wetting a smooth vitreous silica surface. This was confirmed in the experimental studies of Blake (10) and Ingram (11) on the wetting of α-alumina and silica by n-alkanes.

A much more complicated fluid is water. Even though gold has a very high energy surface, it has been demonstrated that water does not wet uncontaminated gold (12). After considerable research, the following explanation has been deveoped in the literature (12, 13). Since water is polar, $\gamma_\ell \neq \gamma_\ell^d$. Instead, $\gamma_\ell = 0.0728\ J/m^2$, and $\gamma_\ell^d = 0.0218\ J/m^2$. In addition, for gold, $\gamma_s^d = 0.121\ J/m^2$. Using Eq. (III.16), the theoretical contact angle is 65.5° which has been confirmed experimentally (12). Therefore, the polar nature of water and its attraction for itself prevents water from wetting uncontaminated gold. A further complication occurs when the gold surface is oxidized. In this cause, the surface becomes hydrophilic because there is a larger dipole-dipole force of interaction between the metal oxide and the water. The above discussion concerning water has been included to emphasize the increased complexity introduced by the presence of strong permanent dipoles. A further complication can occur in the

case of "autophobic liquids", which are liquids that cannot spread on adsorbed oriented monolayers of their own vapor (14). In this case, the adsorbed oriented molecules form a film whose critical surface tension to wetting is less than the surface tension of the liquid itself. In addition to these effects it is always possible to have a contaminated surface. For example, a thin layer of adsorbed water vapor can drastically alter the wetting properties of a high surface energy material for hydrocarbons.

In summary we can say that, although the interline region is very complicated, sufficient theoretical models are available to describe the interline region. However, it is difficult to know the exact experimental conditions at the interline. Therefore, unless an effort is made to fully characterize an experimental heat transfer surface inconsistencies in the heat transfer and contact angle data will be prevalent.

III.4 Representative Values of $[\varepsilon(i\xi) - 1]$

Equation (III.4) demonstrates that a thin wetting film of adsorbed liquid on a solid surface will be stable if the dielectric constant of the solid along the imaginary frequency axis is greater than that of the liquid, $\varepsilon_s(i\xi) > \varepsilon_\ell(i\xi)$. Therefore, it is instructive to compare the values of $\varepsilon(i\xi)$ for various materials. In Fig. (III.1), the $\log_{10} [\varepsilon(i\xi) - 1]$ is presented as a function of the energy associated with an electromagnetic wave in electron volts, $\log_{10} (h\xi)$. In general, $\varepsilon(i\xi)$ decreases monotonically from $\varepsilon_o = \hat{n}^2 > 1$ (for dilectries) or $+\infty$ (for ideal metals) at $\omega = i0$ to 1 at $\omega = i\infty$. The source of the individual values are given in Appendix A.

For non-polar dielectric materials the static dielectric constant, ε_o, can be obtained using the Maxwell relation, $\varepsilon_o = n^2$, in which the index of refraction, n, can be obtained in the visible range of frequencies. It is a measure of the induced polarization. The n-alkanes and diatomic molecules are representative of these materials. Curves for pentane and helium are presented in Fig. (III.1). For comparison, limiting values of nitrogen, oxygen, methane and carbon-tetrafluoride are also given.

Polar molecules have in addition to the induced polarization an orientation polarization. As a result the dielectric constant is not constant in the frequency range below the visible. The alcohols and water are representative of this group. The curve for water in Fig. (III.1) stops at $h\xi \approx 1$. At $\xi = 0$, the dielectric constant for water has a value of $\varepsilon_o = 81$. At $h\xi = 3.16$, $\varepsilon \simeq 1.75$. At most frequencies the dielectric constant for pentane is less than that for water. Experimentally, pentane has been observed to form a thin wetting film on a water substrate (15). Films of octane on water are marginally stable. A theoretical study of hydrocarbon adsorption on water surfaces that describes and confirms this phenomenon has been done using Lifshitz's theory (16).

The values of $\varepsilon(i\xi)$ for ideal metals (smooth and clean surfaces free from oxides and contaminates) are also presented in Fig. (III.1). Since the complex part of the dielectric constant, 2n k, is large for metals, $\varepsilon(i\xi)$ also has a relatively large value. In practical heat transfer equipment these values cannot be reached since non-idealities (oxides and adsorbed contaminates) are usually present. However they do represent an upper limit for $\varepsilon(i\xi)$. Experimentally, the important value is the measured value of $2nk = \varepsilon''$ which characterizes the surface being used. These results also emphasize the fact that metals are high energy surfaces which are easily wetted and easily contaminated.

The dielectric properties of polytetrafluoroethylene (Teflon) fall above but close to those of pentane. Pentane wets Teflon since its surface tension ($\gamma^d = 0.016$ J/m^2) is less than the critical surface tension for the wetting of Teflon (0.0185) J/m^2). From a more fundamental point of view, pentane wets Teflon because $\varepsilon(i\xi)$ for pentane is less than $\varepsilon(i\xi)$ for Teflon. High energy diamond and graphite surfaces have also been studied extensively and the resulting data for $\varepsilon(i\xi)$ are presented in Fig. (III.1).

Although glass is usually considered to be a high surface energy material, the van der Waals interaction constant for glass turns out to be close to those of typical polymer surfaces (17). Therefore, the dielectric properties are not presented in Fig. (III.1). This is confirmed experimentally since the wettability of untreated glass surfaces is poor (18). However, the surface characteristics and wettability of glass surfaces can be changed by various treatments (18). As a result, the surface history (cleaning and preparation) of the glass surface has a considerable influence on the experimentally determined contact angle and many apparent inconsistencies are present in the literature.

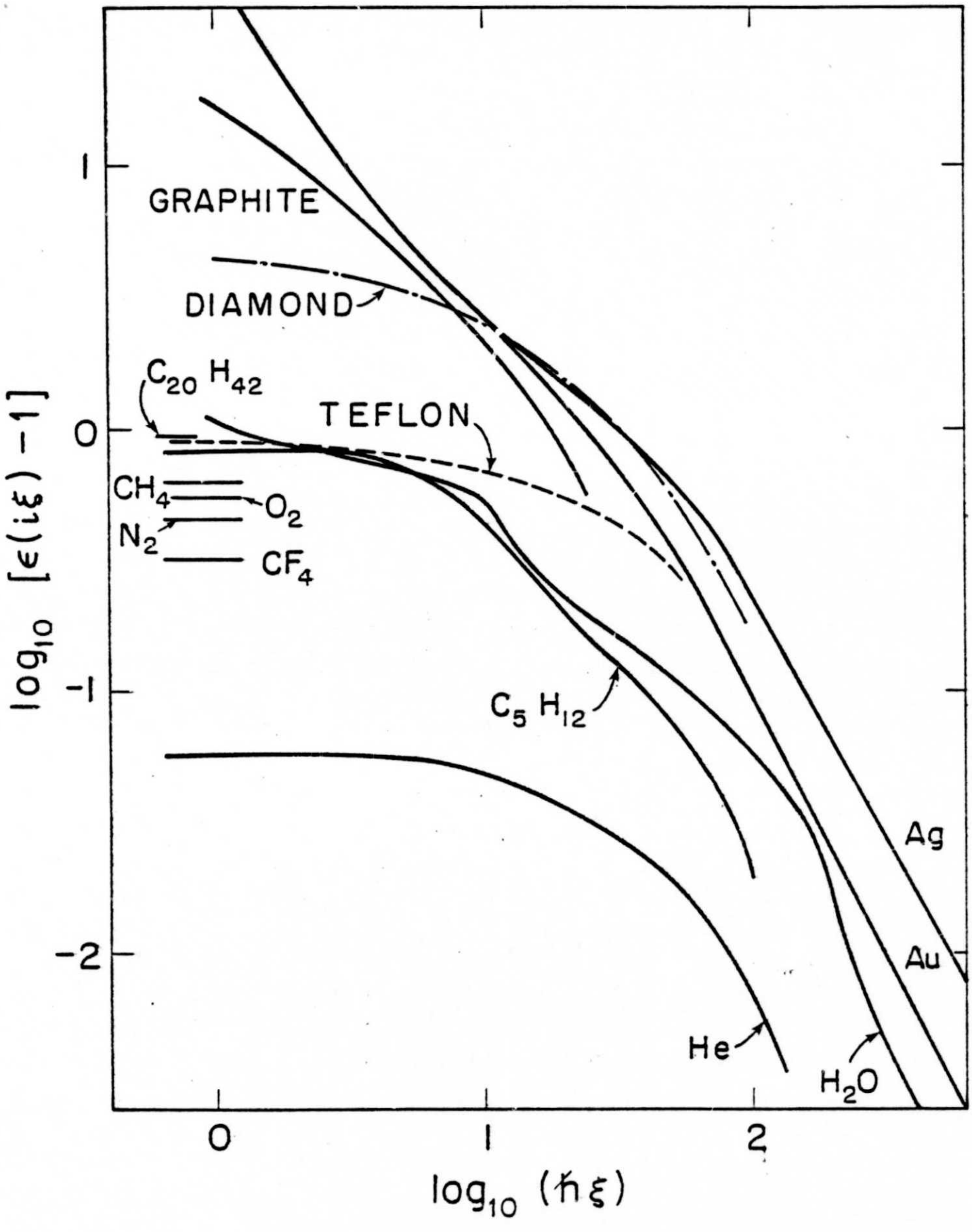

FIGURE (III.1) Plot of $\log_{10}[\epsilon(i\xi)-1]$ as a function of $\log_{10}(\hbar\xi)$ for various materials.

III.5 Theoretical Values of the Hamaker Constant, $A_{s\ell v}$

Churaev used Eq. (III.4) to calculate the Hamaker constant for various systems (22). These results are presented in Table (III.1). Since the dielectric constants for metals are larger than that for water which, in turn, is larger than that for pentane, the absolute value of the Hamaker constants for the pentane - metal systems are larger than that for the pentane - water system. For comparison the Hamaker constant for the He - CaF_2 system is $A_{s\ell v} \tilde{-} 3.8 \times 10^{-21}$ J. (20). The lower values of the dielectric constants for Helium and CaF_2 result in a relatively low value of $A_{s\ell v}$. The refractive index of CaF_2 is approximately $n \tilde{} 1.4$.

The approximate value of the Hamaker constant, $A_{s\ell v}$, can be obtained using

$$A_{s\ell v} = A_{\ell\ell} - A_{s\ell} \qquad \text{(III.19)}$$

A good approximation for the Hamaker constant, $A_{s\ell}$, is $(A_{ss}\ A_{\ell\ell})^{0.5}$ (23). Therefore we can calculate $A_{s\ell v}$ from the more readily available values of A_{ss} and $A_{\ell\ell}$. Calculated values for $A_{s\ell v}$ obtained using Eq. (III.19) are presented in Table (III.2). The values for $A_{\ell\ell}$ were obtained using

$$A_{\ell\ell} = 24\pi\ D^2\gamma \qquad \text{(III.20)}$$

Israelachvili (24) successfully compared the surface tension of a number of saturated hydrocarbons calculated on the Basis of Eq. (III.20) with experimental data. The value for gold was obtained from Ref. (23) and that for Teflon from Ref. (17). In Table (III.3) a list of values for A_{ss} for other solids from these references is given. Graphs of Eq. (III.19) are presented in Fig. (III.2) for various solids: Au, $A_{ss} = 4.5 \times 10^{-19}$ J ; $A\ell_2\ O_3$, $A_{ss} = 1.5 \times 10^{-19}$ J; polystyrene, $A_{ss} = 0.65 \times 10^{-19}$ J. The values for A_{ss} were obtained in Ref. (23).

Due to limitations in the availability and interpretation of the optical data there is a degree of uncertainty in the values of these constants. For example, the curve for $A_{ss} = 1.05 \times 10^{-19}$ J represents the value for Teflon obtained by Vassilieff and Ivanov (17). Their value for Polystyrene is $A_{ss} = 1.11 \times 10^{-19}$ which is considerably different from the value $A_{ss} = 0.652 \times 10^{-19}$ J referenced above (23). As a result of these inconsistencies, the theoretical results based on these initial values of the Hamaker constant are obviously approximate. However, the relative values calculated using the same set of assumptions are very instructive. The refinement of the procedures and the availability of more extensive optical data will lead to more consistent results in the future. The potential use in heat transfer will be an added stimulus for obtaining more extensive optical data.

Table (III.1)

Calculated Values of $A_{s\ell v}$ for Wetting Films (22)

Liquid, substrate	$-A_{s\ell v} \cdot 10^{20}$ J	Liquid, substrate	$-A_{s\ell v} \cdot 10^{20}$ J
Water on quartz	1.12	Pentane on water	0.74
Octane on quartz	1.67	Hexane on water	0.63
Decane on quartz	1.57	Decane on water	0.34
Tetradecane on quartz	1.34	Octane on steel	19.2
Benzene on quartz	0.91	Decane on steel	18.9
$C C\ell_4$ on quartz	0.56	Decane on gold	23.1
		Water on gold	11.2

Table (III.2)

Values of A_{slv} Calculated Using Eq. (III.19)

$A_{ss} \cdot 10^{20}$ J	$A_{\ell\ell} \cdot 10^{20}$ J	$-A_{slv} \cdot 10^{20}$ J
Gold : 45	Methane : 3.95	9.4
Gold : 45	Pentane : 5.04	10.0
Gold : 45	Hexane : 5.48	10.2
Gold : 45	Heptane : 5.82	10.4
Gold : 45	Octane : 6.08	10.5
Gold : 45	n•Dodecane : 6.75	10.7
Gold : 45	Nitrogen : 2.49	8.1
Teflon : 10.5	Methane : 3.95	2.5
Teflon : 10.5	Octane : 6.08	1.9
Teflon : 10.5	Nitrogen : 2.49	2.6

Table (III.3)

Calculated Values of A_{ii} from Ref. (17)

Material	$A_{ii} \cdot 10^{20}$ J	Material	$A_{ii} \cdot 10^{20}$ J
Decane	6.7	Poly propylene	9.05
Diamond	41.4	Teflon	10.5
Hydrocarbon II	7.7	Quartz	8.65
Polyethylene	10.5	Water	6.05
Polystyrene	11.1		

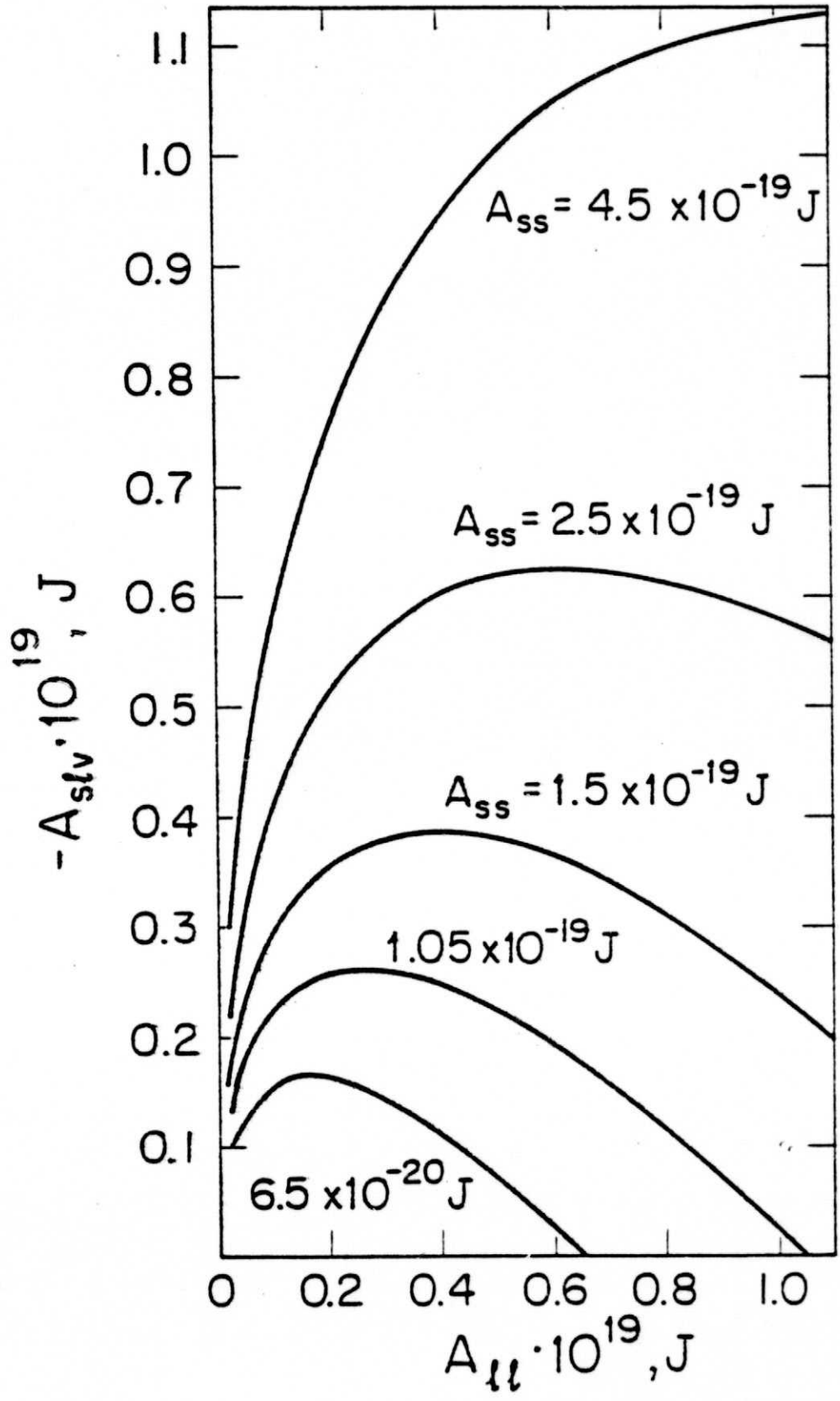

FIGURE (III.2) Calculated value of the Hamaker constant for a thin film of liquid on a solid substrate (Eq. III.19).

III.6 Theoretical Values of the Interline Heat Flow Number, $\bar{A}\, h_{fg}/\nu$

The product of the surface transfer coefficient, $\bar{A}/\nu$, and the heat of vaporization, h_{fg}, gives a measure of the interline heat sink capability of the liquid - solid system, which we call the Interline Heat Flow Number, $h_{fg}\, \bar{A}/\nu$. For the constant heat flux model, the average heat flux over the meniscus thickness range $\eta > 1$ is obtained using (Eq. II.15c)

$$\bar{q} = \frac{1}{x^2} \frac{\bar{A}\, h_{fg}}{\nu} \; 2\, \ell\, \eta \quad . \tag{III.20}$$

The lower limit for the length of the thin film, x, of thickness range, $\eta > 1$, depends on meniscus stability and is beyond the scope of this study. Assuming bulk values for the heat of vaporization and the kinematic viscosity, the interline heat flow number can be calculated using the values for $\bar{A} = -A_{s\ell v}/6\pi$ previously obtained. Theoretical values for the interline heat flow number for a few representative systems are presented in Table (III.4). The gold-alkane system and the Teflon-alkane system are two ideal systems for comparison since the solids have been extensively studied and the alkanes are simple non-polar fluids. More importantly, these systems represent a broad range since gold is a very high surface energy material and Teflon is a very low surface energy material. The value of the interline heat flow number for methane-gold is 9.76×10^{-9} W versus 2.6×10^{-9} W for methane-Teflon. Increasing the molecular weight of the fluid gives $h_{fg}\, \bar{A}/\nu = 2.62 \times 10^{-9}$ W for octane-gold versus 0.26×10^{-9} W for octane-Teflon. This decrease occurs because the ratio h_{fg}/ν decreases faster than $\bar{A}$ increases. For all practical purposes these numbers bracket the range for simple fluids. The inconsistencies present in the table values for the interline heat flow number result from the inconsistencies in the values of $\bar{A}$ in the literature in the different references. For

a finite contact angle system, the "interline region" as defined herein vanishes and the meniscus starts with a finite thickness. Polar fluids and liquid metals are not addressed herein.

Table (III.4)

Theoretical Values of Interline Heat Flow Number, $h_{fg} \bar{A} \nu^{-1}$

Liquid - Substrate	$(h_{fg} \bar{A} \nu^{-1}) \cdot 10^{9}$ Watts		$\bar{A}$ Source
Methane - Gold	9.76	(111.4K) (1)	Table (III.2)
Pentane - Gold	5.26	(293K)	Table (III.2)
Hexane - Gold	4.22	(293K)	Table (III.2)
Heptane - Gold	3.33	(293K)	Table (III.2)
Octane - Gold	2.62	(293K)	Table (III.2)
Do decane - Gold	1.12	(293K)	Table (III.2)
Nitrogen - Gold	4.17	(77K)	Table (III.2)
Decane - Steel	2.90	(293K)	Ref. (22)
Decane - Steel	4.14	(447K) (2)	Ref. (22)
Decane - Gold	3.50	(293K)	Ref. (22)
Methane - Teflon	2.60	(111.4K)	Table (III.2)
Octane - Teflon	0.26	(293K)	Table (III.2)
Nitrogen - Teflon	1.53	(77K)	Table (III.2)
C $C\ell_4$ - Quartz	0.105	(293K)	Ref. (22)
C $C\ell_4$ - Quartz	0.497	(350K) (2)	Ref. (22)
Octane - Quartz	0.418	(293K)	Ref. (22)

(1) h_{fg} and ν are evaluated at this temperature.

(2) Ref. (22) values for $\bar{A}$ were adjusted for temperature using Eqs. (III.19 and III.20).

IV. The Theoretical Interline Heat Sink, Q

The above results can be used to estimate various characteristics of the interline evaporation process. The theoretical interline heat sink for a unit length of interline, Q, is obtained using

$$Q = \bar{q}\, x = [2\ \ell n\ \eta]^{0.5}\ [\bar{q}]^{0.5}\ [h_{fg}\bar{A}/\nu]^{0.5} \qquad \text{(IV.1)}$$

The length of the interline region of thickness range $\eta > 1$, x, is

$$x = [2\ \ell n\ \eta]^{0.5}\ [\bar{q}]^{-0.5}\ [h_{fg}\bar{A}/\nu]^{0.5} \qquad \text{(II.13)}$$

These equations are presented in Figs. (IV.1 and IV.2) for $\eta = 10$. In Fig. (IV.1) some of the values of $\bar{A}h_{fg}/\nu$ listed in Table (III.4) are marked on the theoretical curve. Obviously an increase in the interline heat flow number gives an increase in the theoretical heat sink, Q, and the length of the interline region, x. Two of the systems, decane-steel and carbon tetrachloride-glass are given in more detail in Fig. (IV.2). Curve (1a) represents the decane-steel system at 293K and Curve (1b) represents the system at 447K. Curve (2) represents the carbon tetrachloride system at 293K. The results predict that the interline heat sink, Q, for the decane-steel system is approximately three times larger than that for the carbon tetrachloride system at the same heat flux and $P_v = 1.01 \times 10^5\ N{\cdot}m^{-2}$. This results from the increased length of the evaporating thin film, x, of thickness $1 < \eta \leq 10$, which is a function of the interline heat flow number. The increase of Q with temperature results from the substantial decrease in the kinematic viscosity in this temperature range. This increase will not continue since the dispersion constant will decrease substantially at higher temperatures. For the carbon tetrachloride-quartz system, both the dispersion constant and the reciprocal of the kinematic viscosity increase with temperature at this temperature level (note the effect of the relative size of

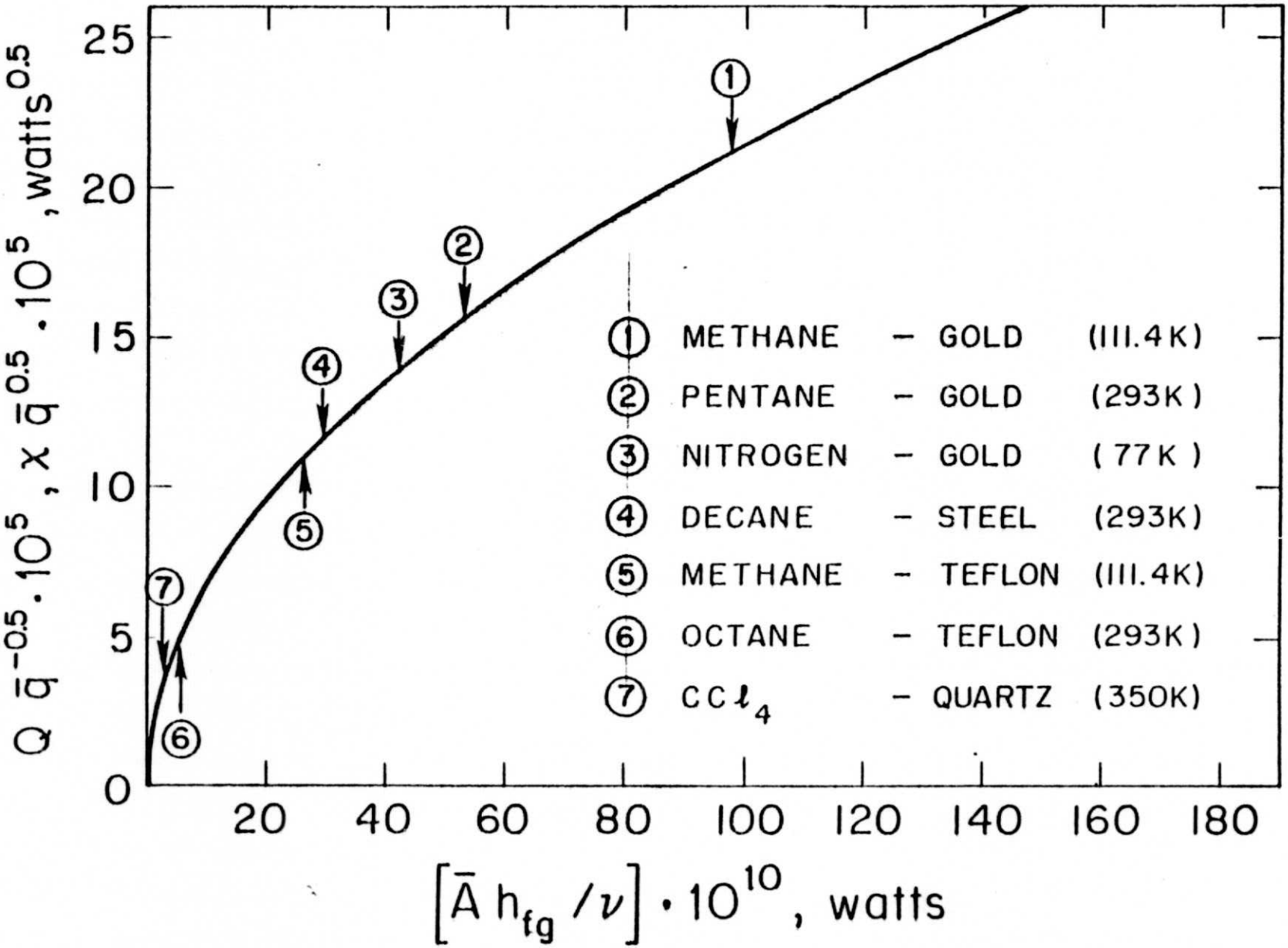

FIGURE (IV.1) Graphical representation of Eq. (IV.1) and Eq. (IV.2).

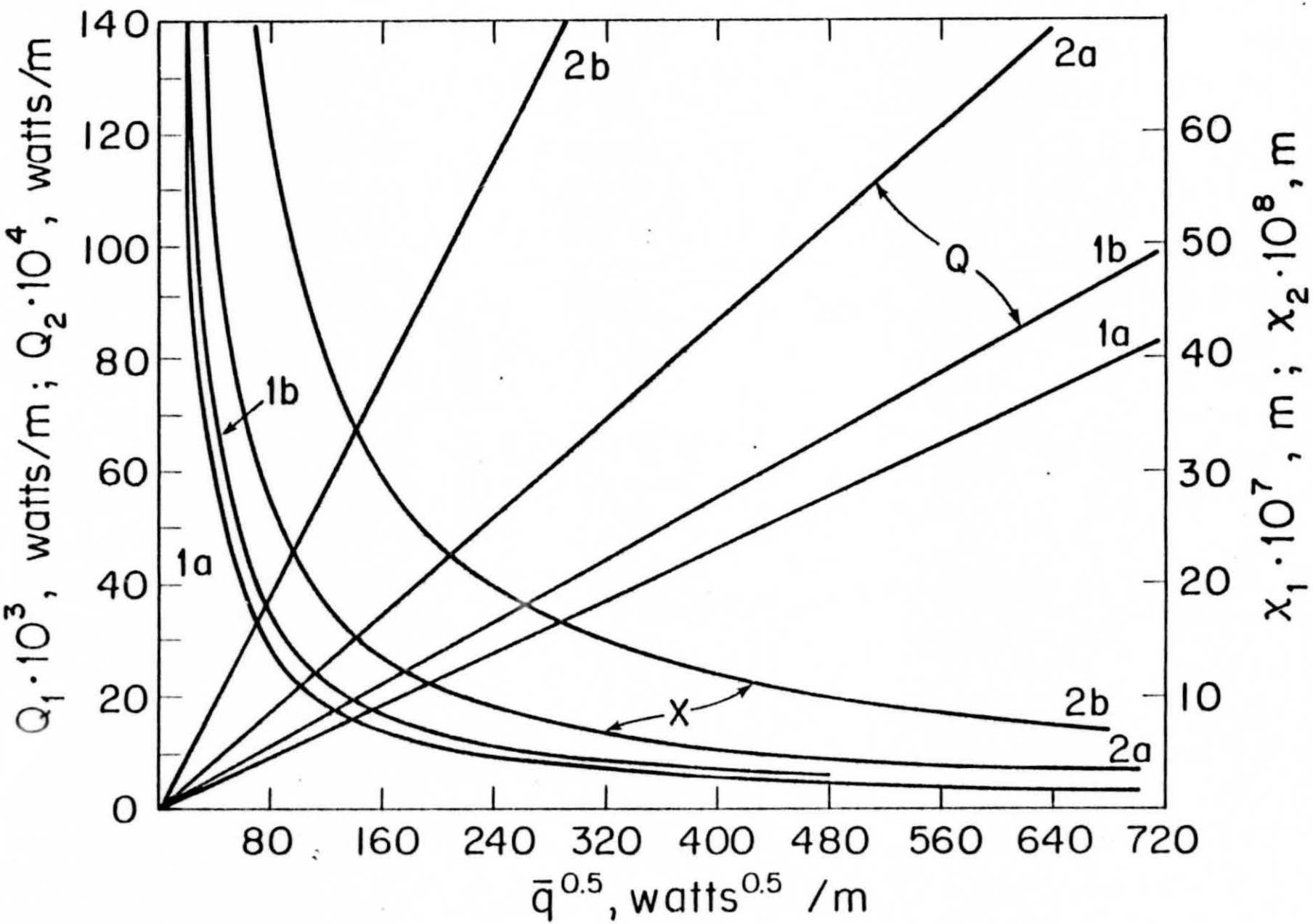

FIGURE (IV.2) Heat sink capability, Q, and interline length, x, for n = 10: (1a) decane-steel at 293K; (1b) decane-steel at 447K; (2a) $CC\ell_4$ - quartz at 293K; (2b) $CC\ell_4$ - quartz at 350K.

A_{ii} on $A_{s\ell v}$ in Fig. (III.2)).

For a more extensive numerical example we compare the heat transfer characteristics of an evaporating thin film of carbon tetrachloride on quartz with those of decane on steel in Table (III.5). The size of the ideal heat flux is approximately fixed by the vapor pressure and temperature difference for all practical purposes. Therefore, it is desirable to compare the two systems at the same vapor pressure level for which we use the atmospheric pressure of 1.01×10^5 $N \cdot m^{-2}$. Although this is desirable from a heat transfer point of view, it does add an additional uncertainty since the extrapolated values of $\bar{A}\, h_{fg}\, \nu^{-1}$ presented in Table (III.4) are used. The interline temperature difference of 10^{-2}K is used to fix the heat flux level at approximately $\bar{q} = 16{,}000$ $W \cdot m^{-2}$. Due to the larger value of $\bar{A}$, the interline thickness, δ_o, and the interline length, x, of the decane system are larger than those of the carbon tetrachloride system. This gives the decane system a higher heat sink capability, Q. The larger values of the interline heat flow number and the thermal conductivity of the solid combine to give the decane-steel system a much larger effective overall heat transfer coefficient, U_{eff}. For comparison, the heat transfer characteristics are also given for $T_v = 293$K. Although it is not possible to predict the maximum stable heat flux at the present time, the larger values of $\bar{A}$ and δ_o for the decane-steel system should also give a larger maximum stable heat flux.

Since the constant heat flux model, Eq. (II.2), does not include a unique value of the liquid-solid interfacial temperature difference at the interline, $(T_{\ell v} - T_v)_0$, the same numerical results can be obtained using Eqs. (II.13) and (II.15) with a different set of interline conditions. For example, keeping η and $\bar{q}$ unchanged, the same numerical results obtained in Table (III.5) for x and Q with $CC\ell_4$-quartz can be obtained using $\bar{\gamma} = 0.05$ and $(T_{\ell v} - T_v)_0 = 0.1$. In this example, the average interfacial temperature difference which is fixed by the

Table (III.5)

Comparison of Carbon Tetrachloride-Quartz System with the Decane-Steel System

	$C\,C\ell_4$ - Quartz T_v = 293K	$C_{10}H_{22}$ - Steel T_v = 293K	$C_{10}H_{22}$ - Steel T_v = 447.2K	$C\,C\ell_4$ - Quartz T_v = 349.7K
$\delta_o \cdot 10^{10}$, m	29	103	121	45
$G \cdot 10^{-10}$, m^{-2}	7,000	6.4	800	6,560
$h_{\ell v}^{id} \cdot 10^{-4}$, $W \cdot m^{-2} \cdot K^{-1}$	74	1.85	330	326
$\bar{A} \cdot 10^{22}$, N·m	3	100	66	7.7
$\frac{h_{fg}\,\bar{A}}{\nu} \cdot 10^{10}$, W	1.05	29	41.4	4.97
$P_v \cdot 10^{-4}$, $N \cdot m^{-2}$	1.19	0.012	10.1	10.1
$\bar{q}^{id} \cdot 10^{-4}$, $W \cdot m^{-2}$	0.74	0.0186	3.3	3.26
$\bar{q} \cdot 10^{-4}$, $W \cdot m^{-2}$	0.37	0.0093	1.65	1.63
$\bar{\gamma}$	0.5	0.5	0.5	0.5
η	10	10	10	10
$Q \cdot 10^{3}$, $W \cdot m^{-1}$	1.34	1.12	17.5	6.19
$x \cdot 10^{6}$, m	0.36	12	1.05	0.38
$U_{eff} \cdot 10^{4}$, $W \cdot m^{-1} \cdot K^{-1}$	3.10	2,040	179.8	3.17
S, m	10^{-3}	10^{-3}	10^{-3}	10^{-3}
$(T_s - T_v)$, K	≈2.85	≈0.0036	≈0.65	≈12.7
$(T_{\ell v} - T_v)_o$, K	0.01	0.01	0.01	0.01

heat flux, $(T_{\ell v} - T_v) = \bar{q}/\bar{h}_{\ell v}$, is also unchanged. However, the film thickness range becomes $14 \leq \delta \leq 140\text{Å}$ instead of $29 \leq \delta \leq 290\text{Å}$. Therefore, $\bar{\gamma}$ is a measure of the temperatue change along the solid surface in the immediate vicinity of the interline which is not included in the constant heat flux model. The constant temperature model demonstrates that a large percent of this temperature change occurs in the thickness range $1 \leq \eta \leq 2$. Which, in turn, indicates that the average heat flux, $\bar{q}$, fixes the average value of $(T_{\ell v} - T_v)$ at approximately its ideal value except in the region $1 \leq \eta \leq 2$. In this region the local temperature gradient with $(T_{\ell v} - T_v)_0 > (T_{\ell v} - T_v)$ fixes δ_0.

V. Discussion

A theoretical procedure to determine the interline heat sink capability of an evaporating meniscus using the macroscopic optical properties and the thermophysical properties of the system has been outlined above. This procedure significantly increases our understanding of the interline and shows how the interline transport processes are controlled by the dispersion forces resulting from the interaction of the solid and liquid. The procedure can be used to predict the relative size of the interline heat sink and, thereby, enhance the development of heat transfer equipment which use the evaporating meniscus and/or the interline region.

Due to the basic nature of the equations, their current level of development and the limited availability of optical data, the use of ideal systems (e.g. neglecting surface roughness) has been emphasized. However, this does not detract from the significance of the results since ideal systems give an order of magnitude approximation and enhanced understanding of real systems, and reveal the basic mechanisms involved in the transport processes.

The constant heat flux model explicitly demonstrated the importance of the interline heat flow number. Using theoretical values of the interline heat flow number, the relative size of the interline heat sink and the interline heat transfer coefficient can be determined. The absolute upper limit of the interline heat sink cannot be determined using only these procedures because the important question of meniscus stability, which must be evaluated experimentally, has not been addressed herein. However, these concepts do describe why the interline heat sink of a system like decane-steel should be greater than that of a system like carbon tetrachloride-quartz. A procedure is now available whereby various systems can be theoretically compared.

By necessity, there are aspects of the above theoretical results which need experimental evaluation, refinement and extension because of the

assumptions in the models. These results indicate that this can be accomplished by measuring the meniscus stability and the interline length, x, as a function of heat flux and the interline heat flow number.

Appendix A

Determination of Values of $\varepsilon(i\xi)$ Used in Fig. (III.1)

There are various procedures to obtain spectral graphs of $\varepsilon(i\xi)$ from the limited experimental data. One of the most useful makes use of the following empirical formula (19)

$$\frac{\varepsilon(i\xi) - 1}{\varepsilon(i\xi) + 1} = a \exp(-b\xi) \qquad \text{(A-1)}$$

This equation was used to obtain the curves for graphite, diamond and Teflon presented in Fig. (III.1). The constants and references are given in Table (A.1).

The curve for pentane was obtained from Ref. (16). The dielectric constant is essentially constant ($\varepsilon = n^2$) from zero frequency through to an ultraviolet frequency, ω_{uv}, which they choose to be the first ionization potential. For frequencies less than ω_{uv} they used the following equation:

$$\varepsilon(i\xi) = 1 + \frac{n^2 - 1}{1 + (\xi/\omega_{uv})^2} \qquad \text{(A-2)}$$

For frequencies higher than the plasma frequency, ω_p, they used Eq. (A.3) with straight line interpolation in between

$$\varepsilon(i\xi) = 1 + \omega_p^2/\xi^2 \qquad \text{(A-3)}$$

The curve for Helium was obtained from Ref. (20) in which a similar procedure was used.

The data for nitrogen, oxygen, methane and carbon tetrafluoride was obtained using

$$\varepsilon = n^2 \qquad \text{(A-4)}$$

and standard values for the index of refraction. The values for gold and silver were obtained from Ref. (21).

Table (A.1)

Constants and References for Eq. (A.1)

Substance	a	$b \cdot 10^{17}$, s/rad	Ref.
Graphite	0.948	3.9	19
Diamond	0.705	1.5	17
Polyethylene	0.420	2.1	17
Polypropylene	0.390	2.1	17
Teflon	0.317	1.2	17
Polystyrene	0.433	2.1	17

References

1. G. Preiss and P. C. Wayner, Jr., Evaporation From a Capillary Tube, Trans A.S.M.E. J. Heat Trans. 96, 178 - 181 (1976).

2. P. C. Wayner, Jr., Y. K. Kao and L. V. LaCroix, The Interline Heat-Transfer Coefficient of an Evaporating Wetting Film, Int. J. Heat Mass Transfer 19, 487 - 491 (1976).

3. B. Chu, Molecular Forces, Interscience Publishers, New York, N.Y. (1967).

4. H. C. Hamaker, Physica (Utrecht) 4, 1058 (1937).

5. I. E. Dzyaloshinskii, E. M. Lifshitz and L. P. Pitaevskii, The General Theory of Van der Waals Forces, Adv. Physics 10, 165 - 208 (1959).

6. A. Sheludko, Colloid Chemistry, Elsevier Pub. Co., New York, N.Y. (1966).

7. L. D. Landau and E. M. Lifshitz, Electrodynamics of Continuous Media, pp. 247 - 268, Pergamon Press, New York, N.Y. (1960).

8. T. Young, Phil. Trans. Royal Soc. (London) 95, 65 1805).

9. F. M. Fowkes, Symposium Chairman, Contact Angle, Wettability and Adhesion, Adv. in Chem. Ser. No. 43, American Chemistry Society, Washington, D.C. (1969).

10. T. D. Blake, Investigation of Equilibrium Wetting Films of n-Alkane on α-Alumina, J. Chem. Soc., Faraday Trans. I 71, 192-208 (1974).

11. B. T. Ingram, Wetting of Silica by n-Alkanes, J. Chem. Soc., Faraday Trans. I 70, 868-876 (1974).

12. R. A. Erb, Wettability of Metals under Condinuous Condensing Conditions, J. Phys. Chem. 69, 1307-1310 (1965).

13. E. Thelen, Dispersion Energies and Surface Tensions of Noble Metals, J. Phys. Chem. 71, 1946-1948 (1967).

14. W. A. Zisman, Relation of the Equilibrium Contact Angle to Liquid and Solid Constitution, (in Twenty Years of Colloid and Surface Chemistry, The Kendall Award Addresses, Edited by K. J. Mysels, C. S. Samour and

J. H. Hollister), American Chemical Society, Washington, D.C. (1973).

15. F. Hauxwell and R. H. Ottewill, A. Study of the Surface of Water by Hydrocarbon Adsorption, J. Colloid Interface Sci. 34, 473 (1970).

16. P. Richmond, W. Ninham and R. E. Ottewill, A Theoretical Study of Hydrocarbon Adsorption on Water Surfaces Using Lifshitz Theory, J. Colloid Interface Sci. 45, 69-80 (1973).

17. Chr. St. Vassilieff and I. B. Ivanov, Simple Semiempirical Method of Calculating van der Waals Interactions in Thin Films from Lifshitz Theory, Zeit. für Naturforsch. 31a, 1584-1588 (1976).

18. G. Alexander and G.A.F.M. Rutten, Surface Characteristics of Treated Glasses for the Preparation of Glass Capillary Columns in Gas-Liquid Chromatography, J. of Chromatography 99, 81-101 (1974).

19. H. Krupp, Particle Adhesion Theory and Experiment, Advan. Colloid Interface Sci. 1, 111-239 (1967).

20. P. Richmond and B. W. Ninham, Calculations of van der Waals Forces Across Films of Liquid Helium Using Lifshitz Theory, Journal of Low Temperature Physics 5, 177-189 (1971).

21. V. M. Muller and N. V. Churaev, Use of the Macroscopic Theory of Molecular Forces to Calculate the Interaction of Particles in a Metal Hydrosol, Kolloidnyi Zournal 36, 492-497 (1974).

22. N. V. Churaev, Molecular Forces in Wetting Films of Non-Polar Liquids, Kolloidnyi Zhurnal 36, 323-327 (1974).

23. H. Krupp, H. Schnabel and G. Walter, The Lifshitz-van der Waals Constant, Computation of the Lifshitz-van der Waals Constant on the Basis of Optical Data, J. Colloid and Interface Sci. 39, 421-423 (1972).

24. J. N. Israelachvili, van der Waals Dispersion Force Contribution to Works of Adhesion and Contact Angle on the Basis of Macroscopic Theory, J. Chem. Soc., Faraday Trans. II 69, 1729-1738 (1973).